Predicting Activation Enthalpies of Cytochrome-P450-Mediated Hydrogen Abstractions. 2. Comparison of Semiempirical PM3, SAM1, and AM1 with a Density Functional Theory Method

Arthur N. Mayeno,*[,†,‡] Jonathan L. Robinson,[†,‡,§] Raymond S. H. Yang,[†,‡] and Brad Reisfeld[†,‡,§]

Quantitative and Computational Toxicology Group, Department of Environmental and Radiological Health Sciences, and Department of Chemical and Biological Engineering, Colorado State University, Fort Collins, Colorado 80523

Received October 23, 2008

Predicting the biotransformation of xenobiotics is important in the chemical and pharmaceutical industries, as well as in toxicology. Here, we extend and evaluate the rapid methodology of Korzekwa, Jones, and Gillette (*J. Am. Chem. Soc.* **1990**, *112*, 7042−7046) to estimate the activation enthalpy ($\Delta H^{\ddagger}$) of hydrogen-abstraction by cytochrome P450 (CYP) enzymes, using the *p*-nitrosophenoxy radical (PNPO) as a simple surrogate for the CYP active oxygen species. The $\Delta H^{\ddagger}$ is estimated with a linear regression model using the reaction enthalpy and ionization energy (of the substrate radical) as predictor variables, calculated by semiempirical (SE) methods. While Korzekwa et al. used the SE method AM1, we applied PM3 and SAM1 and compared the results of the three methods. For 24 substrates, the AM1-, PM3-, and SAM1-derived regression models showed R^2 values of 0.89, 0.90, and 0.93, respectively, for the correlation between calculated and predicted $\Delta H^{\ddagger}$. Furthermore, we compared the $\Delta H^{\ddagger}$ calculated semiempirically using PNPO radical with density functional theory (DFT) B3LYP activation energies calculated by Olsen et al. (*J. Med. Chem.* **2006**, *49*, 6489−6499) using a more realistic iron−oxo−porphine model, and the results revealed limitations of the PNPO radical model. Thus, predictive models developed using SE predictors provide rapid and generally internally consistent results, but they should be interpreted and used cautiously.

INTRODUCTION

The cytochromes P450 (CYP) are a superfamily of enzymes that mediate phase I biotransformations, primarily acting as a monooxygenase, where an oxygen atom is incorporated into substrates.[1−3] This process usually detoxifies hydrophobic xenobiotics but also bioactivates certain substrates, via transformation into electrophilic species capable of interacting with biological molecules.[2,4,5] The rates and regioselectivity of CYP-mediated metabolism influence the importance of various biotransformation pathways, affect the abundance of certain potentially toxic or pharmacologically active metabolites, and alter the clearance characteristics of chemicals. Thus, the ability to predict product regioselectivity and rates can provide insights into assessing the risks and pharmacological efficacy of xenobiotics.

Prediction of metabolism by CYP enzymes has been the subject of intense research for a number of decades,[6−11] especially in recent years as computational methods have improved in speed and accuracy. Attempts to predict rates and regioselectivity of CYP reactions have proven difficult because of multiple confounding factors, including the promiscuity (broad substrate specificity)[12] of CYP enzymes toward substrates, the existence of multiple CYP isoforms and their allelic variants (polymorphism),[13] the allosteric behavior[14−17] of some CYP isozymes, the difficulty in obtaining 3-D (crystal) structures of the isozymes until recently,[18] the possible presence of multiple forms of the active oxygen species within CYP (e.g., iron–oxo, hydroperoxy−iron, peroxo−iron),[19−21] and its spin multiplicity (high and low spin states).[22−24] The recent elucidation of the tertiary structure of several human CYP isozymes (CYP1A2, 2A6, 2A13, 2C8, 2C9, 2D6, 2E1, 2R1, 3A4, 7A1, 46A1)[18] has provided insights into the active sites. Approaches to predicting biotransformations have been categorized into four classes by Zhou et al.:[25] (1) quantum chemical calculations of substrates or of reactions utilizing simplified surrogates for the iron−oxo complex, (2) molecular docking combined with scoring functions, (3) probabilistic scoring method based on fragment analysis of the substrates, and (4) GRID molecular interaction fields describing ligand−protein interactions. Other researchers cluster in silico regioselectivity prediction methodologies into three classes: (1) rule-based, (2) quantitative structure−activity relationship (QSAR), and (3) mechanism-based.[11] Regardless of the classification schemes, the general consensus is that accurate prediction of metabolism requires consideration of both the intrinsic reactivity of each site within the substrate and the contribution of the CYP active site in orienting the substrate relative to the active oxygenating species.[26]

The active oxygenating species that can be used to rationalize most CYP-generated metabolites is the porphyrin−iron−oxo form, called Compound I (Cpd I), and also denoted as "FeO^{3+}".[27] Transition state geometries and

* Corresponding author phone: 970-491-8929; fax: 970-491-7569; e-mail: arthur.mayeno@colostate.edu.
† Quantitative and Computational Toxicology Group.
‡ Department of Environmental and Radiological Health Sciences.
§ Department of Chemical and Biological Engineering.

10.1021/ci8003946 CCC: $40.75
Published on Web 06/12/2009

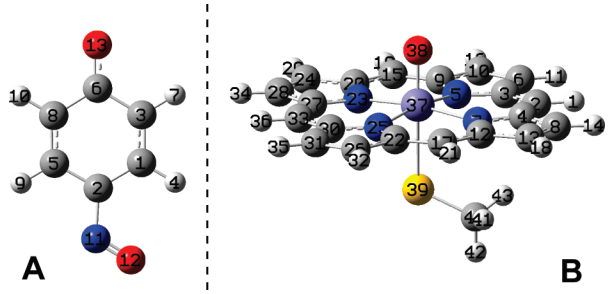

Figure 1. Structures of models used for Cpd I: (A) PNPO Radical, (B) $OFePorSCH_3$. Reactive oxygen is no. 13 and no. 38 for A and B, respectively. AM1 and DFT B3LYP optimized, respectively.

energies of some substrates and Cpd I have been calculated using density functional theory (DFT)[22,23,28] and wave function approaches,[29−31] but a drawback of these methodologies is the calculation time and the exacting procedures required to locate a transition state or states. An approach by Korzekwa et al.[32] and Jones et al.[33] to rapidly predict rates and regioselectivity of CYP-mediated hydroxylation utilizes the semiempirical quantum mechanical Austin Model 1 (AM1) method and the *p*-nitrosophenoxy radical (PNPO) (Figure 1A) as a surrogate model for Cpd I in aliphatic hydroxylation,[32,34] and the methoxy radical as the surrogate in aromatic hydroxylation.[35] More recently, Olsen et al.,[26] using DFT calculations with a more realistic Cpd I model ($OFePorSCH_3$) (Figure 1B), showed that the AM1 method with simple Cpd I surrogates, such as PNPO, can reasonably reproduce DFT results in estimating hydrogen-abstraction activation energies. The corroboration of the semiempirical approaches with DFT is important in that semiempirical calculations can offer a computational speed advantage of orders of magnitude over wave mechanical and DFT methods but with a potential sacrifice in accuracy. These methodologies focus on the intrinsic reactivity of substrates and would be applicable for CYPs where substrate-active site interactions are not a major contributor in orientation, such as those CYPs with larger active sites and for substrates of similar structure, where such interactions would be similar among the substrates.

Here, we extend and evaluate the pioneering work of Korzekwa et al.[32] and Jones et al.[33] to predict relative rates of CYP-mediated alkyl hydroxylation, by using semiempirical Parametric Method 3 (PM3)[36] and Semi ab initio Model 1 (SAM1).[37,38] PM3 is a semiempirical methodology similar to AM1 but with a different parametrization approach,[36] while SAM1[37,38] is a more recent semiempirical approach, implemented in the commercial software package AMPAC. First, results from each of the semiempirical methods were used to create linear regression equations relating the activation enthalpy to the heat of reaction and the ionization potential (IP) of the intermediate carbon-centered radical, based on 24 substrates (Figure 2) studied by Olsen et al.[26] Predictions from our new model equations were consistent with those of Korzekwa et al.,[32] although some notable differences were observed among the AM1, PM3, and SAM1 results. Then, each of the semiempirically calculated and predicted activation enthalpies using the PNPO model were compared with the DFT-derived activation energies using the more realistic iron−oxo−porphine model reported by Olsen et al.[26]

COMPUTATIONAL METHODS

Semiempirical AM1, PM3, and SAM1 quantum mechanical calculations were performed using AMPAC 8.16 (Semichem Inc., Shawnee Mission, KS) with Agui 8.16 (GUI; Semichem Inc., Shawnee Mission, KS); in addition, AM1, PM3, and DFT calculations were performed using Gaussian 03 (G03),[39] version 6.1 for Windows (Gaussian, Inc., Wallingford, CT), with GaussView 4.1[40] (Semichem, Inc., Shawnee Mission, KS), on a Dell Precision workstation, with two quad core Intel Xeon Processors, X5460, 3.16 GHz, and 8 GB RAM (3GB usable with Windows XP, 32-bit), or on the Colorado State University Center for Bioinformatics Cluster, consisting of an Apple G5 cluster of 32 Xserve G5 nodes, with each node containing dual 2.3 GHz PowerPC G5 CPUs and 8 GB memory (64 CPUs total).

Geometry Optimization. The calculation approach was similar to that of Korzekwa et al.[32] and Jones et al.[35] For computational details, see Supporting Information. All calculations were for the gas phase. Each SE TS structure was verified by the presence of only one imaginary frequency and by an intrinsic reaction coordinate (IRC) calculation. The unrestricted Hartree−Fock (UHF) and restricted HF (RHF) formalism were used for open-shell and closed-shell systems, respectively. Specific issues regarding calculations are described in the sections below.

PNPO Radical. All three semiempirical methods generated two stable geometries of the PNPO radical, differing primarily in the geometry of the nitroso group. The existence of two AM1-calculated PNPO conformers was not reported by Korzkewa et al.[32] or Olsen et al.[26] For SAM1 TS determinations, both conformations of the PNPO radical were evaluated (see Results and Discussion); however, for AM1 and PM3 TS determinations, the lower energy PNPO radical was used because (i) the higher energy PNPO geometry converted to the lower energy geometry during the TS determination process (e.g., at the start of the reaction path, during the TS conformational analyses, or during TS optimization) or (ii) convergence problems were encountered during TS optimization for all substrates.

DFT Calculations. For our DFT results, final energies were calculated at the B3LYP/6-311++G(2d,2p) level, using B3LYP/6-31G(d) geometries, and include the thermal correction to enthalpy at 298.15 K (which incorporates the zero-point vibrational energy, ZPE).[41] The unrestricted formalism (UB3LYP) was used for open-shell systems. ZPEs were calculated at the B3LYP/6-31G(d) level, and the thermal correction included a scale factor of 0.9804,[41] calculated via the Freq(ReadIsotopes) keyword option in G03. The thermal correction to enthalpy at 298.15 K was calculated to facilitate comparison of the DFT enthalpy with that calculated using AMPAC, which is parametrized to experimental ΔH_f at 298 K.[42] G03 default convergence criteria were used, unless otherwise noted. Extensive DFT conformational analyses of the PNPO radical, using UB3LYP with the basis sets 6-31G(d), 6-311+(3df), and 6-311G++(2d,2p), revealed only a single global energy minimum geometry for the PNPO radical.

Terminology and Statistical Analyses. In the text, values are given as the mean ± standard deviation, unless otherwise noted. All stable geometries and transition states were verified by the presence of zero and one imaginary frequency,

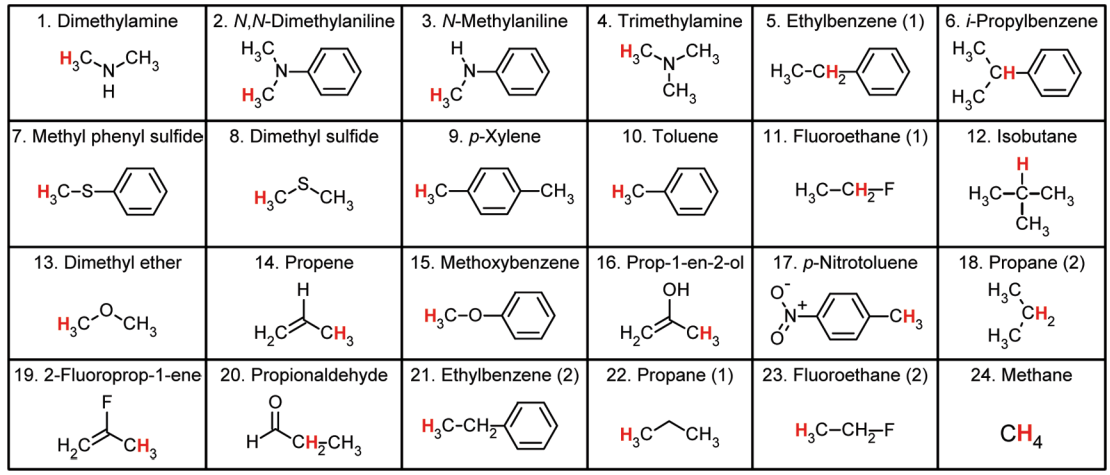

Figure 2. Substrate structures. The location of the hydrogen abstracted is indicated in bold red and, where appropriate, by a number in parentheses after the name.

respectively. "Calculated" refers to values determined via computational chemistry, while "estimated" and "predicted" refer to those determined by regression methods. "Mean absolute difference" (MAD) refers to the average of the unsigned pairwise differences. When a substrate name is followed by a number in parentheses, the number indicates the carbon from which the hydrogen is abstracted. Statistical analyses of regression models were performed using R software (www.r-project.org).

RESULTS AND DISCUSSION

Comparison of Semiempirical AM1, PM3, and SAM1 Calculations for PNPO Reactions: Energies and Ionization Potentials. We used the 24 substrates (Figure 2) studied by Olsen et al.[26] and determined the transition state energies and geometries using AM1, PM3, and SAM1. For the determination of the transition state structure, rotational conformations were exhaustively evaluated, and the lowest energy transition state structure with one imaginary frequency was selected.

The activation enthalpies ($\Delta H^{\ddagger}$) were calculated for the reaction between the PNPO radical and each of the 24 substrates, after the transition state structure was determined using AM1, PM3, and SAM1 (Figure 3; Supporting Information, Tables S1−S3). For ease of comparison, the substrates are arranged in order of ascending AM1 $\Delta H^{\ddagger}$, as was done by Korzekwa et al.[32] To verify that our methods were consistent with those of Olsen et al.,[26] we compared our AM1 $\Delta H^{\ddagger}$ (Supporting Information, Table S1) and TS geometries (Supporting Information, Table S4) with their AM1 results; overall, our data were identical or very similar, except for the substrate *p*-nitrotoluene (Supporting Information, Table S5). (For a thorough analysis of AM1, PM3, and SAM1 TS geometries, see Supporting Information.)

Figure 3 shows that the calculated AM1 and PM3 $\Delta H^{\ddagger}$ values were generally similar or nearly identical (mean absolute difference, MAD = 1.4 ± 0.9 kcal/mol); the largest absolute and relative differences occurred for the amines and sulfides, with the PM3 method giving larger $\Delta H^{\ddagger}$ values than AM1. Dimethylamine showed the largest difference of 22.8 vs 25.8 kcal/mol; abs. diff. = 3.0, rel. diff. = 12.3% [= 3.0/mean (22.8, 25.8)]. Propionaldehyde and hydrocarbons isopropylbenzene, isobutane, ethylbenzene (2), and

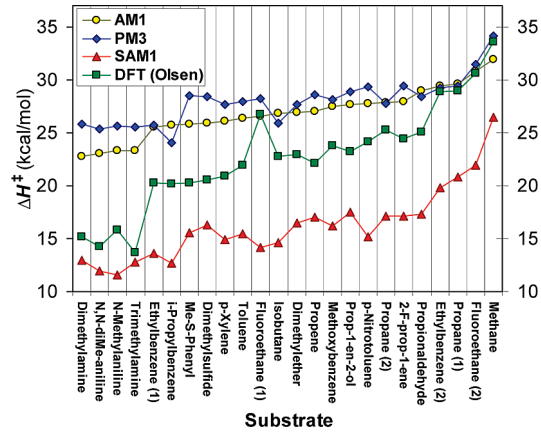

Figure 3. Activation enthalpies ($\Delta H^{\ddagger}$) calculated from AM1, PM3, and SAM1 transition state and reactant structures for the reaction, PNPO• + H−R → [PNPO···H···R]. DFT activation energies from Olsen et al.[26] are also shown. Number in parentheses indicates carbon from which hydrogen is abstracted.

propane, on the other hand, showed slightly larger values using AM1. The $\Delta H^{\ddagger}$ range for calculated AM1 was 22.8 kcal/mol (dimethylamine) to 32.0 kcal/mol (methane); for PM3, 24.1 kcal/mol (isopropylbenzene) to 34.1 kcal/mol (methane).

SAM1 activation enthalpies using the higher energy PNPO radical (Figure 3), however, were all smaller than their corresponding AM1 and PM3 values: SAM1 vs AM1 MAD = 10.6 ± 1.6 kcal/mol; SAM1 vs PM3 MAD = 11.7 ± 1.7 kcal/mol. SAM1 $\Delta H^{\ddagger}$ values also exhibited a wider range (from 11.6 kcal/mol for *N*-methylaniline to 26.5 kcal/mol for methane) than either AM1 or PM3. Thus, all of the calculated AM1 and PM3 $\Delta H^{\ddagger}$ were greater than 22 kcal/mol, while most of the SAM1 $\Delta H^{\ddagger}$ were below 20 kcal/mol, except for methane (26.5 kcal/mol), fluoroethane (2) (22.0 kcal/mol), and propane (1) (20.8 kcal/mol). In Figure 3, the activation energy pattern observed for SAM1 results mimicked PM3 more so than AM1.

The enthalpy of reaction (ΔH_{rxn}), for PNPO abstraction of a hydrogen atom from a substrate to give the phenol and the substrate radical (PNPO• + H−R → PNPOH + •R), was calculated from the lowest energy conformation of each substrate, substrate radical, PNPO, and PNPOH, for AM1 and PM3 (Figure 4). For SAM1, both the lower- and higher-

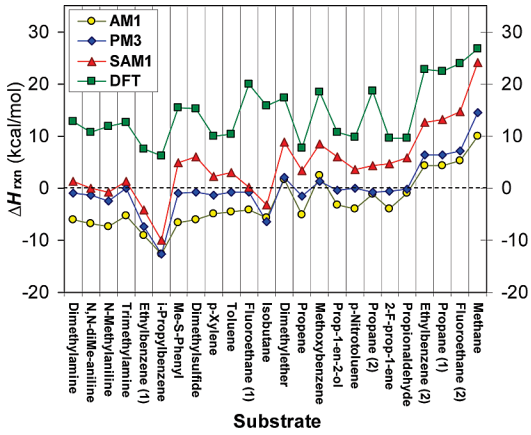

Figure 4. AM1, PM3, SAM1, and DFT ΔH_{rxn} for the reaction of PNPO radical and substrate, giving PNPOH and substrate radical (PNPO + H−R → PNPOH + •R). DFT model chemistry is described in Supporting Information, Table S6.

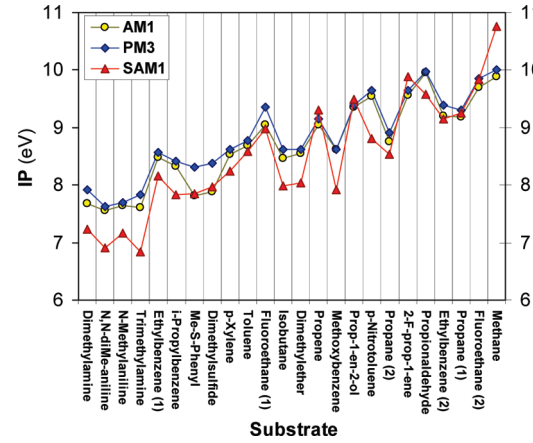

Figure 5. AM1, PM3, and SAM1 ionization potential for the substrate radical (•R)

energy PNPO radical were examined, with the results using the higher energy PNPO shown in Figure 4. The calculated AM1 heats of reaction were exothermic for most of the substrates (except dimethyl ether, methoxybenzene, ethylbenzene (2), propane (1), fluoroethane (2), and methane), while PM3 reactions were approximately thermoneutral for most of the listed substrates.

Quantitatively, the AM1 ΔH_{rxn} were usually more exothermic than the PM3 values (MAD = 3.0 ± 1.9 kcal/mol), while SAM1 values were consistently more endothermic than their respective AM1 and PM3 results by a MAD of 7.5 ± 2.7 kcal/mol and 4.7 ± 2.3 kcal/mol, respectively. This endothermic shift in SAM1 values can be accounted for by examining the components of Hess's law:

$$\Delta H_{rxn} = [\Delta H_f(\text{PNPOH}) + \Delta H_f(\text{substrate radical})] - [\Delta H_f(\text{PNPO}) + \Delta H_f(\text{substrate})] \quad (1)$$

$$= [\Delta H_f(\text{PNPOH}) - \Delta H_f(\text{PNPO})] + [\Delta H_f(\text{substrate radical}) - \Delta H_f(\text{substrate})] \quad (2)$$

The value of [ΔH_f (PNPOH) − ΔH_f (PNPO)] is a constant for each method and is −21.9 kcal/mol for SAM1, −28.7 kcal/mol for AM1, and −26.4 kcal/mol for PM3. As the SAM1 ΔH_{rxn} differs by an average of 7.5 and 4.7 kcal/mol from the AM1 and PM3 ΔH_{rxn}, respectively, the shift in ΔH_{rxn} between SAM1 vs AM1 and PM3 can be largely attributed to this [ΔH_f (PNPOH) − ΔH_f (PNPO)] difference.

Initially, we used the lower energy PNPO conformation for all semiempirical TS determinations, but with SAM1, we were unable to locate TS's for five substrates using the lower energy PNPO conformation (Supporting Information, Table S7 and Figure S1). Thus, we carefully examined conformations of PNPOH and PNPO using AM1, PM3, and SAM1, by varying the dihedral angles H−O−C−C and O−N−C−C, as well as the nitroso O−N−C bond angle. For PNPOH, each method produced two stable structures (i.e., a local and a global energy minimum; Supporting Information, Table S8 and Figure S2), verified by the absence of imaginary frequencies. For the PNPO radical, the conformational analyses revealed that each of the methods also produced two structures, one corresponding to a local energy minimum and another to the global minimum, each confirmed by the lack of imaginary frequencies. The energy of the higher PNPO local minimum structure was 19.0 kcal/mol (AM1), 21.1 kcal/mol (PM3), and 11.3 kcal/mol (SAM1), while that of the global minimum was 14.1, 19.7, and 4.4 kcal/mol, respectively. Use of the higher energy SAM1 PNPO structure allowed us to find TS's for all substrates, with the higher energy PNPO shifting the SAM1 $\Delta H^{\ddagger}$ upward by a nearly constant value of 1.7 ± 0.2 kcal/mol (Supporting Information, Figure S1 and Table S7), excluding the five substrates for which TS structures could not be found.

The ionization potential (IP) of the substrate radical has been used as a quantitative measure of the radical's stability,[32] and because of its ease of calculation (based on Koopmans Theorem)[43,44] may serve a practical and useful descriptor in developing a regression model predicting activation enthalpies. Koopmans' Theorem[44] states that the energy required to remove an electron from an orbital is the negative of the orbital energy (i.e., IP ≈ –highest occupied molecular orbital energy, or $-\varepsilon_{HOMO}$). The AM1-, PM3-, and SAM1-calculated IP of the substrate radicals are shown in Figure 5 and Tables S1, S2, S3. PM3 IP values closely matched AM1 values or were slightly higher (MAD 0.15 ± 0.13 eV), with the sulfide radicals being the only notable exceptions, where IP for methyl phenyl sulfide and dimethyl sulfide were 0.50 and 0.49 eV higher for PM3 than for AM1, respectively. SAM1 IP values were generally lower than both AM1 and PM3 values (MAD of 0.36 ± 0.26 eV and 0.45 ± 0.26 eV, respectively), although radicals of propene, prop-1-en-2-ol, 2-fluoroprop-1-ene, and methane gave higher SAM1 IP values. SAM1 IP for propane (1), fluoroethane (2), and the sulfide radicals rested between the AM1 and PM3 IP.

An important requisite in using the PNPO radical as a surrogate for Cpd I in predicting hydrogen abstraction rates is the existence of a correlation between the calculated [PNPO···H···substrate] activation enthalpy and the true $\Delta H^{\ddagger}$ of the [(Cpd I)···H···substrate] TS. The rationale for using PNPO was based on the evidence that the TS for ω-hydroxylation of aliphatic compounds is symmetrical, and, of the model compounds examined, PNPO produced the most thermodynamically symmetrical ethane/PNPO reaction ($\Delta H_{rxn} \approx 0$) and possessed a symmetrical TS geometry ($r_{CH}/r_{tot} = 0.51$).[32]

The mechanistic basis for the PNPO model is the "oxygen rebound" mechanism proposed by Groves,[45] where $(FeO)^{3+}$

Table 1. Olsen et al.[26] DFT Activation Energy (using $OFePorSCH_3$), Shaik et al.[28] DFT $\Delta E^{\ddagger}$ (using OFePorSH), and Mayeno et al. Semiempirical AM1, PM3, and SAM1 $\Delta H^{\ddagger}$ (using PNPO radical)

		Olsen et al. activation energy ($OFePorSCH_3$)		Shaik et al. $\Delta E^{\ddagger}$ [a] (OFePorSH)		Mayeno et al. calculated $\Delta H^{\ddagger}$ [b] (PNPO)			Mayeno et al. predicted $\Delta H^{\ddagger}$ [c] (PNPO)		
no.	substrate	DFT HS[d] (kJ/mol)	DFT HS[d] (kcal/mol)	DFT HS (kcal/mol)	DFT LS (kcal/mol)	AM1 (kcal/mol)	PM3 (kcal/mol)	SAM1 (kcal/mol)	AM1 (kcal/mol)	PM3 (kcal/mol)	SAM1 (kcal/mol)
1	dimethylamine	31.9	7.62			22.80	25.79	12.92	24.22	26.33	13.35
2	*N*,*N*-dimethylaniline	28.9	6.91	5.54	4.99	23.04	25.39	11.91	23.85	25.80	12.45
3	*N*-methylaniline	31.9	7.62			23.31	25.59	11.61	23.90	25.65	12.59
4	trimethylamine	27.9	6.67			23.31	25.50	12.82	24.19	26.48	12.77
5	ethylbenzene (1)	50.6	12.09	12.55	11.47	25.50	25.74	13.61	25.31	25.70	13.01
6	isopropylbenzene	55.8	13.34			25.74	24.07	12.71	24.34	24.19	10.71
7	methyl (phenyl) sulfide	45.4	10.85			25.84	28.49	15.54	24.40	26.95	15.37
8	dimethyl sulfide	45.9	10.97			25.89	28.43	16.28	24.65	27.07	15.87
9	*p*-xylene	53.0	12.67			26.09	27.66	14.89	26.12	27.31	15.12
10	toluene	54.6	13.05	12.43	12.05	26.41	27.97	15.45	26.51	27.64	15.85
11	fluoroethane (1)	61.6	14.72			26.58	28.24	14.20	27.34	28.56	15.54
12	isobutane	59.7	14.27			26.83	25.95	14.62	25.85	26.05	13.04
13	dimethyl ether	50.9	12.17			26.88	27.69	16.50	27.38	28.12	16.85
14	propene	53.9	12.88	12.95	12.82	27.06	28.55	17.02	27.13	28.02	16.97
15	methoxybenzene	54.5	13.03			27.47	28.15	16.20	27.65	27.94	16.55
16	prop-1-en-2-ol	49.1	11.74			27.69	28.88	17.45	28.10	28.68	18.11
17	*p*-nitrotoluene	49.5	11.83			27.80	29.28	15.19	28.34	29.14	16.32
18	propane (2)	62.0	14.82	15.80	13.85	27.87	27.78	17.09	27.29	27.86	16.16
19	2-fluoroprop-1-ene	55.2	13.19			27.91	29.41	17.10	28.39	29.01	18.30
20	propionaldehyde	47.9	11.45			28.96	28.40	17.32	29.71	29.58	18.14
21	ethylbenzene (2)	72.2	17.26			29.46	29.22	19.82	29.14	30.35	19.66
22	propane (1)	73.9	17.66	17.48	15.19	29.61	29.45	20.82	29.12	30.23	19.96
23	fluoroethane (2)	77.2	18.45			30.85	31.46	21.96	30.33	31.25	21.29
24	methane	86.7	20.72	22.91	22.34	31.96	34.13	26.47	31.57	33.30	25.51
					MAD:[b,c]	14.12	15.22	3.58	14.12	15.22	3.80
					SD:[b,c]	1.71	2.45	1.75	2.21	2.45	1.79

[a] Shaik et al.[28] singlepoint calculations were done on the optimized geometries in Jaguar 7.0 using a triple-ζ quality LACV3P+ basis set on iron and 6-311+G* on the rest of the atoms (basis set B2). The values shown include ZPE, which were taken from the UB3LYP/B1 frequency calculations, where the B1 basis set uses LACVP basis set on iron and a 6-31G basis set on the rest of the atoms. HS = high spin (quartet); LS = low spin (doublet). [b] "Calculated" refers to values determined using TS structure enthalpies. Mean absolute difference (MAD), relative to Olsen et al. data, is listed at the bottom. [c] "Predicted" refers to values determined by regression methods. MAD, relative to Olsen et al. data, is listed at the bottom. [d] HS = high spin (quartet).

abstracts a hydrogen atom in the first step to yield $(FeOH)^{3+}$ and substrate radical, followed by recombination of hydroxyl radical from $(FeOH)^{3+}$ to give the hydroxylated substrate. As recombination has been theoretically verified to be fast, albeit influenced by spin state,[46] the relative rates of hydroxylation are dependent on the activation energy of this initial abstraction step, suggesting that prediction models based on this step are reasonable. Models relating activation enthalpies to heats of reaction derive from the Bell−Evans−Polanyi (BEP) principle,[47,48] which states that a linear relationship may exist between the activation energy and the enthalpy of reaction within a series of closely related reactions, i.e., $E_a = \alpha + \beta \times \Delta H_{rxn}$, where α and β are constants.

Olsen et al.[26] compared the DFT B3LYP activation energies using a more complete Cpd I model with those using the PNPO radical and found good coefficients of determination (R^2) of 0.89 and 0.86, using B3LYP and AM1, respectively, for the PNPO-substrate activation energy. The activation energies calculated by Olsen et al.[26] were consistent with values calculated by Shaik et al. (Table 1).[23,28] These results suggest that PNPO can serve as a rough model for Cpd I, and, assuming that [PNPO···H···substrate] TS is an adequate model for the analogous Cpd I TS, the regression models derived, using the easily calculable descriptors, should provide good estimates of the activation enthalpies.

Linear Regression Models Predicting Activation Enthalpies: AM1 vs PM3 vs SAM1. In an attempt to extend and improve the models of Korzekwa et al.,[32] we developed linear regression models relating activation enthalpy to heat of reaction and ionization potential, using AM1, PM3, and SAM1 data with the substrate set used by Olsen et al.[26] We initially performed AM1 calculations on the 20 substrates studied by Korzekwa et al.[32] and, overall, reproduced their results (data not shown), verifying that our methodology was consistent with theirs. The plot of our AM1-calculated vs predicted (based on our AM1 regression model) enthalpy of activation is shown in Figure 6A. Our model, $\Delta H^{\ddagger}_{pred} = 9.91 + 0.18 \times \Delta H_{rxn} + 2.01 \times IP$, exhibited an R^2 of 0.89, slightly lower than 0.92 reported by Korzekwa et al. (including all substrates). This difference can be attributed to more chemical variation within our substrate set, e.g., the presence of sulfide compounds, whose removal from the regression calculation increases our R^2 value to 0.93. In fact, the largest absolute difference between calculated and predicted $\Delta H^{\ddagger}$ was 1.4 kcal/mol for methyl phenyl sulfide. The span of our AM1 $\Delta H^{\ddagger}$ values was shifted upward relative to that of Korzekwa et al.,[32] with our calculated (and predicted) results

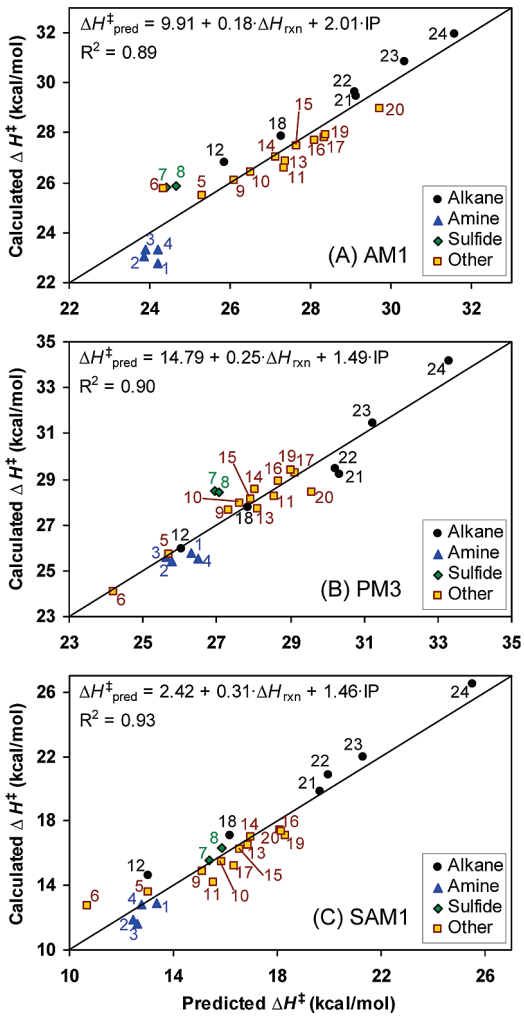

Figure 6. Calculated vs predicted activation enthalpies for hydrogen abstraction with PNPO radical using (A) AM1, (B) PM3, and (C) SAM1. $\Delta H^{\ddagger}_{pred}$ is determined from the linear regression equation with predictors ΔH_{rxn} and ionization potential (IP). The number labels correspond to substrates listed in Figure 2. MAD is 0.63, 0.51, and 0.70 kcal/mol for AM1, PM3, and SAM1, respectively.

ranging from 22.8 to 32.0 kcal/mol (and 23.9 to 31.6 kcal/mol) (Table S1), compared to 16.3 and 27.2 kcal/mol (and 17.2 kcal/mol to 30.9 kcal./mol). This notable shift is largely caused by the 5.0 kcal/mol difference in ΔH_f of the PNPO radical values, where we used the lower energy conformer (14.1 kcal/mol), while Korzekwa et al. used the higher energy conformer (19.0 kcal/mol). In a subsequent publication, they used the lower energy of PNPO.[34]

As shown in Figure 6A, the AM1-based regression model showed certain trends based on chemical class. Specifically, the model slightly underestimated the activation enthalpies for all alkane substrates, as well as the sulfides and isopropylbenzene, while overestimating the activation enthalpies for all of the amines, relative to the AM1-calculated $\Delta H^{\ddagger}$. Of the chemical classes represented by the substrates, the amines showed the lowest $\Delta H^{\ddagger}$.

The PM3-based regression model of activation enthalpies ($\Delta H^{\ddagger}_{pred} = 14.79 + 0.25 \times \Delta H_{rxn} + 1.49 \times IP$) showed a marginally larger R^2 of 0.90 and a slightly shifted predicted range (24.2 to 33.3 kcal/mol) (Table S2), with a somewhat different spread pattern than the AM1 regression (Figure 6B). For example, unlike the AM1 model, the PM3-derived model did not consistently overestimate the $\Delta H^{\ddagger}$ for the alkanes, and, isopropylbenzene, rather than the amines, displayed the lowest $\Delta H^{\ddagger}$, with this $\Delta H^{\ddagger}$ better predicted by the PM3 regression model. Like the AM1 model, the PM3-derived model overestimated activation enthalpies of the sulfide compounds.

The SAM1-based regression model of activation enthalpies ($\Delta H^{\ddagger}_{pred} = 2.42 + 0.31 \times \Delta H_{rxn} + 1.46 \times IP$) showed a predicted range of 10.7 to 25.5 kcal/mol and an R^2 of 0.93 (Figure 6C; Supporting Information, Table S3), an R^2 higher than both the AM1 and PM3 models. As mentioned above, the range of $\Delta H^{\ddagger}$ calculated using SAM1 was shifted lower relative to that calculated by AM1 and PM3, with the SAM1 range more in accord with high-level DFT calculations using a more realistic Cpd I (vide infra).[23,26,49−53] As observed with the AM1 regression plot in Figure 6A, the SAM1 regression model slightly underestimates the $\Delta H^{\ddagger}$ for all alkanes, as well as for isopropylbenzene. For sulfides, unlike the AM1 or PM3 models, where the $\Delta H^{\ddagger}$ was overestimated, the SAM1 model predictions of $\Delta H^{\ddagger}$ are more internally consistent (i.e., $\Delta H^{\ddagger}_{pred} \approx \Delta H^{\ddagger}_{calc}$) (MAD of 0.3 ± range 0.2 kcal/mol, compared to 1.3 ± range 0.1 kcal/mol and 1.5 ± range 0.1 kcal/mol for AM1 and PM3, respectively). For all three semiempirical methods, methane exhibited the greatest calculated and predicted $\Delta H^{\ddagger}$, a result expected for this series of substrates based on bond dissociation energy.[54−57]

Thus, the general methodology showed good internal consistency across the semiempirical methods: the descriptors calculated by each semiempirical method could be used to predict the $\Delta H^{\ddagger}$ calculated by that model, e.g., AM1-generated descriptors could predict AM1-calculated $\Delta H^{\ddagger}$, as demonstrated by MAD of 0.63, 0.51, and 0.70 kcal/mol for AM1, PM3, and SAM1, respectively (Supporting Information, Tables S1, S2, and S3).

Comparison of Activation Enthalpies Calculated Semiempirically Using PNPO and Calculated by DFT Using an Iron−Oxo−Porphine Model. A major advantage of semiempirical calculations is the speed compared with wave function and DFT methods, while providing accurate geometries and energies for molecules related to those used for parametrization. Because semiempirical methods are parametrized to reproduce energies and geometries of common stable molecules, energies of transition states (and activation energies derived thereof) are likely to be less accurate than reaction energies.[44] Thus, for molecules outside the training sets, accuracy of geometry and, especially, energy require corroboration with experimental data or higher level methods, such as DFT.[44]

Due to these semiempirical limitations, we compared our semiempirically derived PNPO $\Delta H^{\ddagger}$ against DFT calculations with $OFePorSCH_3$. Previously, Olsen et al.[26] had compared the DFT B3LYP activation energies using a more complete Cpd I model ($OFePorSCH_3$, Figure 1B) with those using the PNPO radical and reported good coefficients of determination (R^2) of 0.89 and 0.86, using B3LYP and AM1, respectively, for the PNPO-substrate activation energy. Here, we evaluated the correlation of our AM1-, PM3-, and SAM1-calculated $\Delta H^{\ddagger}$, using PNPO, with their DFT activation energy,[26] using $OFePorSCH_3$ (Figure 7 and Table 1; Supporting Information, Table S9). Initially, we verified that our AM1-calculated PNPO $\Delta H^{\ddagger}$ were consistent with those of Olsen et al.[26] (see Supporting Information, Table S5). Our R^2 between DFT

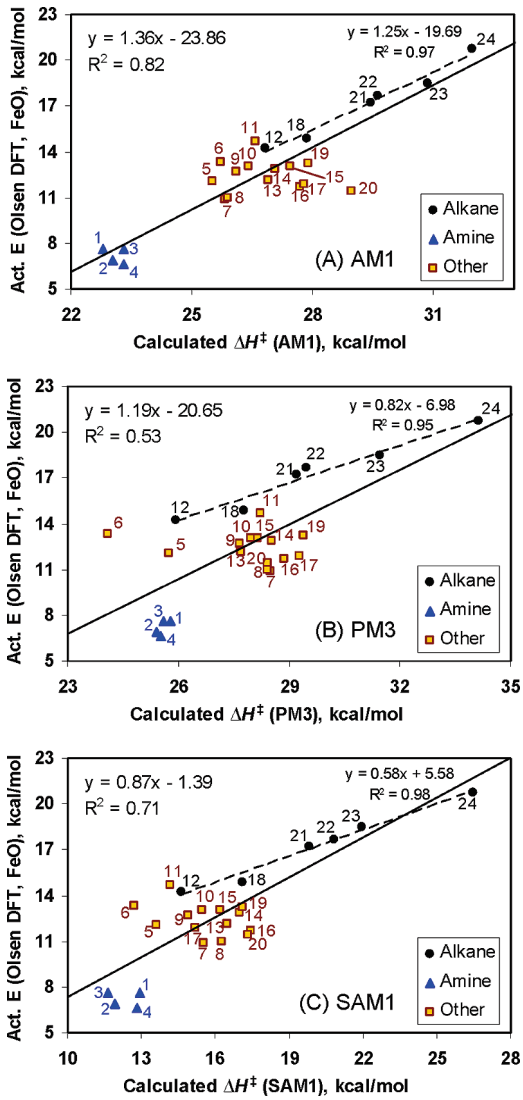

Figure 7. Correlation of DFT activation energy from Olsen et al.,[26] using $OFePorSCH_3$, with our (A) AM1-, (B) PM3-, and (C) SAM1-calculated $\Delta H^{\ddagger}$, using PNPO. The number labels correspond to substrates listed in Figure 2. The dashed line and the solid line represent the least-squares fit using alkanes only and all data points, respectively. The regression equation and R^2 on the upper left includes all points, while the regression equation and R^2 on the upper right includes only the alkanes. MAD is 14.12, 15.22, and 3.58 kcal/mol for AM1, PM3, and SAM1, respectively.

$OFePorSCH_3$ activation energy[26] and AM1 PNPO $\Delta H^{\ddagger}$ was 0.82 (Figure 7), as we used all 24 substrates while the $R^2 = 0.86$ reported by Olsen et al.[26] was based on their training set.

As shown in Figure 7, when comparing the semiempirical PNPO $\Delta H^{\ddagger}$ and DFT $OFePorSCH_3$ activation energy, AM1 showed the highest R^2 while PM3 showed the lowest, with AM1 ($R^2 = 0.82$) > SAM1 ($R^2 = 0.71$) > PM3 ($R^2 = 0.53$). The intercepts of the regression lines were 23.9, 20.6, and −1.4 kcal/mol for AM1, PM3, and SAM1, respectively, indicating that the AM1 and PM3 PNPO methodologies overestimate the activation enthalpies relative to DFT. MADs of 14.1, 15.2, and 3.6 kcal/mol between DFT and AM1, PM3, and SAM1 results, respectively, are consistent with the overestimation of activation enthalpies using SE methods (Table 1; Supporting Information, Table S9).

To evaluate if the correlations showed patterns based on chemical class, we divided the substrates into the following eight classes, based on the substituents attached to the reactive carbon center: alkyl, amino, aryl, carbonyl, halide, oxygen, sulfide, and vinyl. As a class, alkane substrates showed a high correlation between the semiempirically calculated and DFT activation energy (DFT vs: AM1 $R^2 = 0.97$, PM3 $R^2 = 0.95$, SAM1 $R^2 = 0.98$) (Figure 7), although only the regression coefficients (slopes) using AM1 and PM3 were near unity (1.25 and 0.82), while the SAM1 coefficient was 0.58. For all nonalkyl classes, the semiempirically calculated $\Delta H^{\ddagger}$ overestimated the DFT values to a greater extent than for the alkanes. For example, *p*-nitrotoluene $\Delta H^{\ddagger}$ was 11.8 kcal/mol by DFT while it was 27.8, 29.3, and 15.2 kcal/mol, by AM1, PM3, and SAM1, respectively, whereas for ethylbenzene (2) (where H is abstracted from the terminal CH_3), the $\Delta H^{\ddagger}$ was 17.3 kcal/mol by DFT while it was 29.5, 29.2, and 19.8 kcal/mol, by AM1, PM3, and SAM1, respectively. These results suggest that the contribution of the substituents in stabilization of the TS may not be adequately reflected by these semiempirical methods.

Aryl-substituted substrates also tended to show good linearity when the benzyl position possessed two hydrogens (i.e., $Ar-CH_2-X$, X = H or alkyl), with the exception of *p*-nitrotoluene. Interestingly, isopropylbenzene (with H abstracted from the benzylic position) fit along the regression line of alkane class, also suggesting that the aromatic substituent does not dominate in the stabilization of the TS in both DFT and semiempirical methodologies.

Thus, for simple alkanes and alkylbenzenes, semiempirically calculated $\Delta H^{\ddagger}$ using PNPO can serve as a good estimator of the DFT results for $OFePorSCH_3$, once the regression relationships have been determined, especially using AM1 or SAM1 formalisms. For different chemical classes, an additional class-specific (or indicator) variable would be required to enhance the predictive ability of the model, and, further work with additional substrates, along with evaluation of different descriptors, would be necessary to develop optimal regression models. Additionally, configuration interaction (CI) calculations merit exploration.

Prediction of DFT Activation Energies of an Iron−Oxo−Porphine Model Using Linear Regression Models and Semiempirical Descriptors. A major goal is to rapidly and accurately estimate the activation energy of hydrogen abstraction by Cpd I; thus, we examined the relationship between DFT activation energy (using $OFePorSCH_3$[26]) and the semiempirically predicted $\Delta H^{\ddagger}$ using PNPO (Figure 8; Supporting Information, Table S9), where predicted $\Delta H^{\ddagger}$ was determined using the regression equations determined earlier (Figure 6). Like the semiempirically calculated $\Delta H^{\ddagger}$, AM1 showed the highest R^2 while PM3 showed the lowest, with AM1 ($R^2 = 0.64$) > SAM1 ($R^2 = 0.58$) > PM3 ($R^2 = 0.54$), with MAD of 14.12, 15.22, and 3.80 kcal/mol between DFT and AM1, PM3, and SAM1 results (Figure 8; Supporting Information, Table S9). However, the correlation coefficients for the AM1 and SAM1 models were lower than those when $\Delta H^{\ddagger}$ is calculated semiempirically from the TS structures (Figure 7). The lower R^2 is understandable in that, for computational expediency, we are attempting to interrelate disparate models, i.e., different models of the reactive oxygen species (PNPO vs $OFePorSCH_3$), different model chemistries (semiempirical vs DFT), and predicting activation energies from regression models based on rapidly calculable descriptors. Still, as the

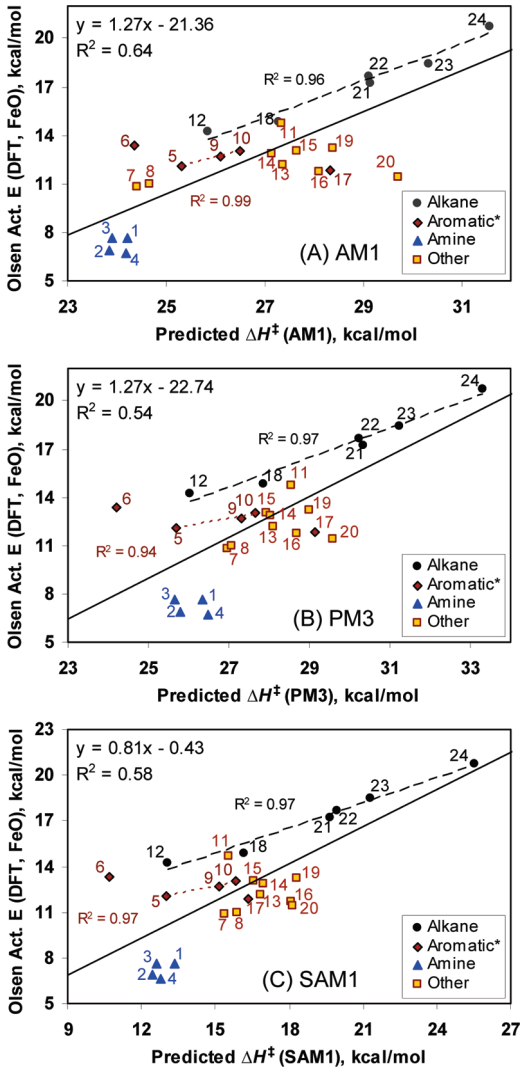

Figure 8. Correlation of DFT activation energy using $OFePorSCH_3$ from Olsen et al.,[26] with our predicted $\Delta H^{\ddagger}$ based on (A) AM1, (B) PM3, and (C) SAM1 linear regression models. The number labels correspond to substrates listed in Figure 2. The solid line represents the least-squares fit using all points. The broken lines represent the least-squares best fit based on alkanes only (black dashed lines) and aromatics (brown dotted lines): *Aromatic regression line excludes *p*-nitrotoluene (substrate no. 17) and isopropylbenzene (substrate no. 6). Isopropylbenzene (substrate no. 6), though not classified as an alkane, fell along the alkane regression line. MAD is 14.12, 15.22, and 3.80 kcal/mol for AM1, PM3, and SAM1, respectively.

semiempirically calculated and predicted $\Delta H^{\ddagger}$ showed a high correlation, similar trends were observed when attempting to predict DFT activation energies using the regression models; for example, the alkanes as a class showed a good linear relationship (R^2 = 0.96, 0.97, 0.97 for AM1, PM3, and SAM1, respectively), while the other classes revealed semiempirically predicted $\Delta H^{\ddagger}$ that were relatively larger compared to the alkanes, i.e., to the right of the alkanes in Figure 8. As mentioned above, further refinement of the model is warranted.

In addition, DFT activation energy from Olsen et al.[26] was regressed against SE ΔH_{rxn} and IP (i.e., we used the semiempirically calculated descriptors, ΔH_{rxn} and IP, based on the PNPO model reaction, to develop linear regression models to predict the Olsen et al.[26] DFT activation energy for $OFePorSCH_3$). These models showed only a minor improvement in R^2 over the linear regression models based solely on the PNPO model, with SAM1 (R^2 = 0.65) > AM1 (R^2 = 0.64) > PM3 (R^2 = 0.61) (Supporting Information, Figure S3 and Table S10; cf. Figures 7 and 8). As expected, the MAD were reduced (as E_a is directly predicted from the SE descriptors) to 1.80, 1.78, and 1.75 kcal/mol between DFT E_a and those predicted from AM1, PM3, and SAM1 descriptors, respectively (Supporting Information, Table S10); again, prediction of alkane E_a demonstrated the highest correlation.

Comparison of Semiempirical Results with Density Functional Theory (DFT) B3LYP Results: DFT Enthalpies of Reaction. To assess the accuracy of semiempirically calculated enthalpies of reaction (ΔH_{rxn}) for hydrogen abstraction by PNPO, we performed DFT calculations on the substrates, substrate radicals, PNPOH, and PNPO, from which ΔH_{rxn} was determined (Figure 4; Supporting Information, Table S6). Energies were determined at the B3LYP/6-311++G(2d,2p) level, at B3LYP/6-31G(d) optimized geometries, and included thermal correction to enthalpy at 298.15 K. DFT-calculated ΔH_{rxn} values were markedly different from those calculated by the semiempirical methods, with the difference increasing from SAM1 (MAD of 9.8 ± 4.4 kcal/mol) to PM3 (MAD of 14.5 ± 3.6 kcal/mol) to AM1 (MAD of 17.3 ± 3.2 kcal/mol) (Figure 4). In Figure 4, for all of the semiempirical methods, the reaction enthalpies tended to increase from left to right and generally exhibited a similar pattern; however, for DFT calculations, the slope was not as pronounced, and the pattern was not consistent with that of any of the semiempirical methods. Moreover, while most of the AM1 and PM3 enthalpies of reaction were exothermic, all of the DFT ΔH_{rxn} were endothermic. Thus, the DFT calculations indicate that the reaction equilibrium lies to the left (i.e., reactants PNPO and substrate). To evaluate the accuracy of ΔH_{rxn} calculated semiempirically and by DFT, we examined ΔH_f (substrate) and ΔH_f (substrate radical) by comparing calculated and experimentally derived bond dissociation energies (vide infra).

Comparison of Semiempirical and DFT Enthalpies of Formation with Experimental Data. The AM1, PM3, and SAM1 enthalpies of formation of substrates (H−R) and substrate radicals (•R) were checked against the available experimental literature data, by comparing the computationally calculated and experimental bond dissociation enthalpy change ($DH°$) for the reaction H−R → H• + •R (Table 2). Our semiempirically calculated $DH°$ revealed notable errors (Table 2); the mean unsigned absolute (and mean unsigned relative) errors were, respectively, 5.1 ± 7.9 kcal/mol (and 5.3 ± 7.6%) for AM1, 7.7 ± 10.6 kcal/mol (and 8.1 ± 10.2%) for PM3, and 9.6 ± 4.8 kcal/mol (and 10.3 ± 5.1%) for SAM1, including calculations for nonsubstrates phenol, *p*-nitrophenol, and the hydrogen molecule. Thus, based on 22 compounds, accuracy followed the order: AM1 > PM3 > SAM1. Examining only the substrates, the error in AM1 $DH°$ appeared random, with amines and sulfides slightly underestimated, while PM3 $DH°$ appeared slightly biased upward. However, SAM1 $DH°$ of the substrates was clearly shifted toward lower values. All of the semiempirical methods overestimated the $DH°$ for phenols (phenol and *p*-nitrophenol), by an average of 9.7%, 11.3%, and

Table 2. Comparison of AM1, PM3, and SAM1 Bond Dissociation Enthalpies (*DH*°), in kcal/mol, with Experimental *DH*° for the Reaction H−R → H• + •R, at 298 K, 1.0 atm

		DH°[a]			*DH*°[b]	*DH*° difference[c]			% error[d]		
no.	substrate	AM1	PM3	SAM1	exptl	AM1	PM3	SAM1	AM1	PM3	SAM1
1	dimethylamine	91.42	97.33	81.79	94.2	2.78	3.13	12.41	2.95	3.32	13.18
2	*N*,*N*-dimethylaniline	90.68	96.95	80.35	91.7	1.02	5.25	11.35	1.11	5.72	12.38
3	*N*-methylaniline	90.12	95.90	79.61							
4	trimethylamine	92.18	98.41	81.75	93.2	1.02	5.21	11.45	1.09	5.60	12.29
5	ethylbenzene (1)	88.52	90.92	76.28	85.4	3.12	5.52	9.12	3.66	6.47	10.68
6	isopropylbenzene	84.96	85.73	70.44	83.2	1.76	2.53	12.76	2.11	3.04	15.34
7	methyl phenyl sulfide	90.98	97.46	85.40	93.0	2.02	4.46	7.60	2.18	4.80	8.17
8	dimethyl sulfide	91.53	97.56	86.44	93.7	2.17	3.86	7.26	2.32	4.12	7.75
9	*p*-xylene	92.55	97.08	82.70	87.7	4.85	9.38	5.00	5.54	10.70	5.70
10	toluene	92.98	97.48	83.45	89.7	3.28	7.78	6.25	3.66	8.68	6.97
11	fluoroethane (1)	93.43	97.66	80.61	98.2	4.77	0.54	17.59	4.85	0.55	17.91
12	isobutane	91.81	91.98	77.22	95.7	3.89	3.72	18.48	4.07	3.89	19.31
13	dimethyl ether	99.24	100.32	89.23	96.1	3.14	4.22	6.87	3.27	4.39	7.15
14	propene	92.46	96.73	83.73	88.2	4.26	8.53	4.47	4.83	9.67	5.07
15	methoxybenzene	99.89	99.62	88.82							
16	prop-1-en-2-ol	94.38	97.93	86.44							
17	*p*-nitrotoluene	93.50	98.28	83.98	86.5	7.00	11.78	2.52	8.09	13.62	2.92
18	propane (2)	96.47	97.58	84.70	98.1	1.63	0.52	13.40	1.66	0.53	13.66
19	2-fluoroprop-1-ene	93.63	97.72	85.22							
20	propionaldehyde	96.62	98.11	86.18	91.7	4.92	6.41	5.52	5.37	6.99	6.02
21	ethylbenzene (2)	101.81	104.73	93.08							
22	propane (1)	101.88	104.71	93.59	100.9	0.98	3.81	7.31	0.97	3.77	7.24
23	fluoroethane (2)	102.88	105.54	95.12	103.6	0.72	1.94	8.48	0.69	1.88	8.18
24	methane	107.57	112.92	104.45	105.0	2.57	7.92	0.55	2.45	7.54	0.52
	phenol	95.80	96.87	103.39	86.7	9.10	10.17	16.69	10.50	11.73	19.25
	p-nitrophenol	99.43	101.26	103.83	91.3	8.13	9.96	12.53	8.90	10.90	13.73
	hydrogen molecule	142.86	157.28	116.95	104.2	38.71	53.13	12.80	37.16	51.01	12.29
mean (excluding hydrogen and all phenols)						2.94	5.08	8.86	3.20	5.54	9.50
SD (excluding hydrogen and all phenols)						1.69	2.98	4.73	1.93	3.42	4.96
mean of the unsigned errors (all compounds above)						5.08	7.72	9.56	5.34	8.13	10.26
SD of the unsigned errors (all compounds above)						7.85	10.61	4.79	7.58	10.23	5.12

[a] *DH*° = ΔH_f (substrate radical) + ΔH_f (H) − ΔH_f (substrate) (see Supporting Information, Tables S1, S2, S3 for values). ΔH_f (H atom) = 68.84, 71.94, 58.55 kcal/mol for AM1, PM3, SAM1, respectively. [b] Experimental *DH*° were taken from Luo;[56] "recommended" values used. For *p*-nitrophenol, *p*-xylene, and *p*-nitrotoluene, *DH*° closest to DFT value was used, as no value was recommended. Blank values indicate experimental *DH*° that were not found. [c] *DH*° Difference = *DH*° (semiempirical) − *DH*° (Luo). [d] % Error = 100 × (*DH*° difference)/(exptl *DH*°).

16.5% for AM1, PM3, and SAM1, respectively. *DH*° for diatomic hydrogen was also overestimated by 37.2%, 51.0%, and 12.3% for AM1, PM3, and SAM1, respectively.

Our AM1, PM3, and SAM1 ΔH_f for substrates are consistent with those previously reported,[36−38,58] although our calculated ΔH_f for radicals were lower, a difference which disappears when we performed configuration interaction (CI) calculations to treat electron correlation (data not shown). We are currently exploring linear regression models based on CI calculations.

The DFT enthalpies of formation of substrates and substrate radicals were similarly checked against experimental data (Table 3). For the substances examined, the DFT-derived *DH*° were all in good agreement with experimental values, though slightly underestimated, with mean unsigned absolute error and mean unsigned relative error of 2.6 ± 1.5 kcal/mol and 2.8 ± 1.6%, respectively. The underestimation of *DH*° (gas phase) using B3LYP for phenolic compounds has been previously reported.[59,60]

These comparisons explain the downward offset of the semiempirical ΔH_{rxn} relative to DFT values in Figure 4. One source of error is the difference between the semiempirical and DFT *DH*° for PNPOH (Supporting Information, Table S11): 21.1 kcal/mol (AM1), 21.9 kcal/mol (PM3), and 4.0 kcal/mol (SAM1, using the higher-energy PNPO radical geometry). All of the semiempirical methods overestimate PNPOH *DH*° relative to DFT (Table S11). Thus, in eq 2, semiempirically, [ΔH_f (PNPOH) − ΔH_f (PNPO)] would be underestimated, leading to smaller ΔH_{rxn}. The other source of error arises from the calculated substrate *DH*° (Table 2): SAM1 considerably underestimates substrate *DH*°, yielding a lower [ΔH_f (substrate radical) − ΔH_f (substrate)] in eq 2. Using dimethylamine as an example, with SAM1, substrate and PNPOH *DH*° error are −12.4 and 4.0 kcal/mol, respectively (Table 2 and above). Adjusting the dimethylamine SAM1 ΔH_{rxn} of 1.3 kcal/mol (Table S3) for these errors gives 17.7 kcal/mol. Because the substrate *DH*° error is relative to experimental *DH*° while PNPOH error is relative to the DFT *DH*°, a factor of 4.9 kcal/mol must be subtracted, affording 12.8 kcal/mol, identical to the DFT ΔH_{rxn} (Table S6).

The cause of the differences in calculated $\Delta H^{\ddagger}$ between SAM1 and AM1/PM3 (Figure 3) is more difficult to assess. The use of the higher energy PNPO radical only partly accounts for the difference. To address this question, we are currently examining transition state calculations of certain PNPO-substrates using DFT.

Table 3. Comparison of DFT and Experimental Bond Dissociation Enthalpies (*DH*°), in kcal/mol, for the Reaction H−R → H• + •R (see footnotes of Supporting Information, Table S6 for computation method)

no.	substrate	DFT *DH*°[a]	exptl *DH*°[b]	difference[c]	% error[d]
1	dimethylamine	89.25	94.2	−4.95	−5.25
2	*N*,*N*-dimethylaniline	87.07	91.7	−4.63	−5.05
3	*N*-methylaniline	88.28			
4	trimethylamine	89.01	93.2	−4.19	−4.50
5	ethylbenzene (1)	83.92	85.4	−1.48	−1.73
6	isopropylbenzene	82.60	83.2	−0.60	−0.72
7	methyl phenyl sulfide	91.93	93.0	−1.07	−1.15
8	dimethyl sulfide	91.76	93.7	−1.94	−2.07
9	*p*-xylene	86.35	87.7	−1.35	−1.54
10	toluene	86.75	89.7	−2.95	−3.28
11	fluoroethane (1)	96.38	98.2	−1.82	−1.86
12	isobutane	92.32	95.7	−3.38	−3.53
13	dimethyl ether	93.66	96.1	−2.44	−2.53
14	propene	84.17	88.2	−4.03	−4.57
15	methoxybenzene	94.85			
16	prop-1-en-2-ol	87.14			
17	*p*-nitrotoluene	86.19	86.5	−0.31	−0.36
18	propane (2)	95.05	98.1	−3.05	−3.11
19	2-fluoroprop-1-ene	86.08			
20	propionaldehyde	86.12	91.7	−5.58	−6.09
21	ethylbenzene (2)	99.13			
22	propane (1)	98.86	100.9	−2.04	−2.02
23	fluoroethane (2)	100.39	103.6	−3.21	−3.10
24	methane	103.20	105.0	−1.80	−1.72
	phenol	83.77	86.7	−2.93	−3.38
	p-nitrophenol	87.90	91.3	−3.40	−3.72
	hydrogen molecule	104.77	104.2	0.62	0.60
mean (all substances listed)				−2.57	−2.76
SD (all substances listed)				1.57	1.70
mean of the unsigned errors (all substances listed)				2.63	2.81
SD of the Unsigned Errors (all substances listed)				1.47	1.60

[a] DFT $DH° = \Delta H_f$ (substrate radical) + ΔH_f (H) − ΔH_f (substrate), thermally corrected and scaled enthalpy (see Supporting Information, Table S6 for values). [b] Exptl *DH*° were taken from Luo.[56] "Recommended" values used. For *p*-nitrophenol, *p*-xylene, and *p*-nitrotoluene, *DH*° closest to DFT value was used, as no value was recommended. Blank values indicate experimental *DH*° were not found. [c] *DH*° Difference = *DH*° (DFT) − *DH*° (Luo). [d] % Error = 100 × (absolute difference)/(exptl *DH*°).

Thus, because reaction enthalpies calculated by semiempirical and DFT methods can differ substantially, semiempirically generated predictors, such as ΔH_{rxn}, must be used cautiously when estimating activation enthalpies.

CONCLUSIONS

Here, we present new semiempirically based models for the rapid prediction of biotransformation of xenobiotics using PNPO as a surrogate. Based on 24 substrates, the regression models derived from each of the semiempirical methods, AM1, PM3, SAM1, showed $R^2 \geq 0.89$ in estimating its calculated activation enthalpy, using ΔH_{rxn} and IP as predictor variables, with SAM1 exhibiting the highest R^2 of 0.93 (Figure 6). The high R^2 values suggest that all of these models are usable and are internally consistent.

The range of estimated $\Delta H^{\ddagger}$ was similar for AM1 and PM3 (Figure 6), but shifted downward for SAM1, with substrates of different chemical classes sometimes ordered differently by the different methods, suggesting that one of the methods may estimate relative activation enthalpies more accurately. The intramethod predictive ability of these models can be improved further by inclusion of an additional variable representing the different classes of substrates, such as alkanes, amines, and sulfides.

The comparison of semiempirically calculated and predicted activation enthalpies, using PNPO, against DFT activation energies calculated by Olsen et al.[26] using a more realistic Cpd I model, revealed limitations; only one class of chemicals, alkanes, showed a high correlation (Figures 7 and 8). The AM1 and PM3 calculated and predicted activation energies require a notable adjustment by a constant factor to bring the values in line with those generated by the SAM1 model and by the more realistic Cpd I model. DFT activation energies regressed directly against AM1, PM3, and SAM1 descriptors only slightly improved the R^2 (Supporting Information, Figure S3). The overall results suggest that semiempirically calculated descriptors, ΔH_{rxn} and IP, could be used in regression models to predict DFT activation energies for alkane substrates with good accuracy, but not necessarily for other chemical classes, with SAM1 yielding the highest R^2 for the set of alkanes evaluated.

Further examination of additional substrates, different predictor variables, and application of different methods, such as configuration interaction, are warranted and may provide better predictive models.

ACKNOWLEDGMENT

We thank Prof. Anthony K. Rappé for helpful discussions. The research was supported, in part, by Grant Number K25ES012909 from the National Institute of Environmental Health Sciences (NIEHS). The content is

solely the responsibility of the authors and does not necessarily represent the official views of NIEHS or the National Institutes of Health.

Supporting Information Available: Additional information on the following are available: TS determination procedures and *p*-nitrosophenoxy radical geometries; Table S1 (AM1 Energies for the Reaction of PNPO Radical with Different Substrates); Table S2 (PM3 Energies for the Reaction of PNPO Radical with Different Substrates); Table S3 (SAM1 Energies for the Reaction of PNPO Radical with Different Substrates When Using the Higher Energy PNPO Geometry); Table S4 (AM1 Transition State Geometries of [PNPO···H···R]); Table S5 (Comparison of AM1 Data from Olsen et al.[26] and Mayeno et al. for the Reaction of PNPO Radical with Different Substrates); Table S6 (DFT Energies of Substrates, Substrate Radicals, and Enthalpies of Reaction); Table S7 and Figure S1 (SAM1 Energies When Starting with the Lower Energy PNPO Radical); Table S8 and Figure S2 (*p*-Nitrosophenol and PNPO Radical Geometries and Energies); Table S9 (Mean Absolute Difference between Olsen et al.[26] DFT Activation Energy Using $OFePorSCH_3$ and Mayeno et al. Semiempirical AM1, PM3, and SAM1 Calculated and Predicted $\Delta H^{\ddagger}$, Using PNPO Radical); Table S10 (DFT Activation Energy, Using $OFePorSCH_3$, from Olsen et al.,[26] Regressed against Semiempirically Calculated Descriptors ΔH_{rxn} and IP); Table S11 (Comparison of Semiempirical and DFT BDE of PNPOH); Table S12 (Differences in Substrate Enthalpies Calculated Using RHF and UHF Wave Functions); Table S13 (PM3 Transition State Geometries of [PNPO···H···R]); Table S14 (SAM1 Transition State Geometries of [PNPO···H···R] Using the Higher Energy PNPO Radical); Table S15 (SAM1 Transition State Geometries When Starting with the Lower Energy PNPO Radical); Table S16 (Comparison of CPU Time for AM1, PM3, SAM1, and G03 DFT B3LYP Calculations for Substrates Methane, Propane, and Dimethylamine); Figure S3 (DFT activation energy for $OFePorSCH_3$, from Olsen et al.,[26] vs activation energy predicted from regression models, where Olsen et al.[26] DFT activation energy was regressed against semiempirical descriptors ΔH_{rxn} and IP); Figure S4 (AM1-, PM3-, and SAM1-calculated ΔH_f of transition state structures [PNPO···H···R]); Figure S5 (Transition state geometries calculated using AM1, PM3, and SAM1 for H-abstraction by PNPO radical); Figure S6 (Calculated AM1, PM3, and SAM1 transition state geometries for hydrogen abstraction by PNPO radical of (A) dimethylamine and (B) propane (1)); Figure S7 (Comparison of transition state geometries of [PNPO···H···substrate] determined by AM1, PM3, and SAM1); Figure S8 (Calculated vs predicted r_{tot} from regression on both ΔH_{rxn} and substrate radical IP, using AM1, PM3, SAM1); Figure S9 (Calculated vs predicted r_{CH}/r_{tot} from regression on both ΔH_{rxn} and substrate radical IP, using AM1, PM3, and SAM1). This material is available free of charge via the Internet at http://pubs.acs.org.

REFERENCES AND NOTES

(1) *Cytochromes P450: Structure, Mechanism and Biochemistry*, 3rd ed.; Ortiz de Montellano, P. R., Ed.; Kluwer Academic/Plenum: New York, 2005.

(2) Parkinson, A. Biotransformation of Xenobiotics. In *Casarett and Doull's Toxicology: The Basic Science of Poisons*, 7th ed.; Klaassen, C. D., Ed.; McGraw-Hill: New York, 2008; pp 161−304.

(3) Brown, C. M.; Reisfeld, B.; Mayeno, A. N. Cytochromes P450: A Structure-Based Summary of Biotransformations Using Representative Substrates. *Drug Metab. Rev.* **2008**, *40*, 1–100.

(4) Guengerich, F. P. Cytochrome P450 Oxidations in the Generation of Reactive Electrophiles: Epoxidation and Related Reactions. *Arch. Biochem. Biophys.* **2003**, *409*, 59–71.

(5) Guengerich, F. P.; Shimada, T. Oxidation of Toxic and Carcinogenic Chemicals by Human Cytochrome P-450 Enzymes. *Chem. Res. Toxicol.* **1991**, *4*, 391–404.

(6) de Groot, M. J. Designing Better Drugs: Predicting Cytochrome P450 Metabolism. *Drug Discovery Today* **2006**, *11*, 601–606.

(7) Crivori, P.; Poggesi, I. Computational Approaches for Predicting CYP-Related Metabolism Properties in the Screening of New Drugs. *Eur. J. Med. Chem.* **2006**, *41*, 795–808.

(8) Madden, J. C.; Cronin, M. T. Structure-Based Methods for the Prediction of Drug Metabolism. *Expert Opin. Drug Metab. Toxicol.* **2006**, *2*, 545–557.

(9) Jolivette, L. J.; Ekins, S. Methods for Predicting Human Drug Metabolism. In *Advances in Clinical Chemistry*; Makowski, G., Ed.; Academic Press: San Diego, 2007; Vol. 43, pp 131−176.

(10) Jung, J.; Kim, N. D.; Kim, S. Y.; Choi, I.; Cho, K. H.; Oh, W. S.; Kim, D. N.; No, K. T. Regioselectivity Prediction of CYP1A2-Mediated Phase I Metabolism. *J. Chem. Inf. Model.* **2008**, *48*, 1074–1080.

(11) Oh, W. S.; Kim, D. N.; Jung, J.; Cho, K. H.; No, K. T. New Combined Model for the Prediction of Regioselectivity in Cytochrome P450/3A4 Mediated Metabolism. *J. Chem. Inf. Model.* **2008**, *48*, 591–601.

(12) Coon, M. J. Multiple Oxidants and Multiple Mechanisms in Cytochrome P450 Catalysis. *Biochem. Biophys. Res. Commun.* **2003**, *312*, 163–168.

(13) Danielson, P. B. The Cytochrome P450 Superfamily: Biochemistry, Evolution and Drug Metabolism in Humans. *Curr. Drug Metab.* **2002**, *3*, 561–597.

(14) Atkins, W. M. Non-Michaelis-Menten Kinetics in Cytochrome P450-Catalyzed Reactions. *Annu. Rev. Pharmacol. Toxicol.* **2005**, *45*, 291–310.

(15) Atkins, W. M. Current Views on the Fundamental Mechanisms of Cytochrome P450 Allosterism. *Expert Opin. Drug Metabol. Toxicol.* **2006**, *2*, 573–579.

(16) Hlavica, P.; Lewis, D. F. V. Allosteric Phenomena in Cytochrome P450-Catalyzed Monooxygenations. *Eur. J. Biochem.* **2001**, *268*, 4817–4832.

(17) Sligar, S. G.; Denisov, I. G. Understanding Cooperativity in Human P450 Mediated Drug-Drug Interactions. *Drug Metab. Rev.* **2007**, *39*, 567–579.

(18) Protein Data Bank. http://www.rcsb.org (accessed March 31, 2009).

(19) Coon, M. J. Cytochrome P450: Nature's Most Versatile Biological Catalyst. *Annu. Rev. Pharmacol. Toxicol.* **2005**, *45*, 1–25.

(20) Newcomb, M.; Hollenberg, P. F.; Coon, M. J. Multiple Mechanisms and Multiple Oxidants in P450-Catalyzed Hydroxylations. *Arch. Biochem. Biophys.* **2003**, *409*, 72–79.

(21) Newcomb, M.; Chandrasena, R. E. P. Highly Reactive Electrophilic Oxidants in Cytochrome P450 Catalysis. *Biochem. Biophys. Res. Commun.* **2005**, *338*, 394–403.

(22) Meunier, B.; De Visser, S. P.; Shaik, S. Mechanism of Oxidative Reactions Catalyzed by Cytochrome P450 Enzymes. *Chem. Rev.* **2004**, *104*, 3947–3980.

(23) Shaik, S.; Kumar, D.; de Visser, S. P.; Altun, A.; Thiel, W. Theoretical Perspective on the Structure and Mechanism of Cytochrome P450 Enzymes. *Chem. Rev.* **2005**, *105*, 2279–2328.

(24) Shaik, S.; Hirao, H.; Kumar, D. Reactivity Patterns of Cytochrome P450 Enzymes: Multifunctionality of the Active Species, and the Two States-Two Oxidants Conundrum. *Nat. Prod. Rep.* **2007**, *24*, 533–552.

(25) Zhou, D. S.; Afzelius, L.; Grimm, S. W.; Andersson, T. B.; Zauhar, R. J.; Zamora, I. Comparison of Methods for the Prediction of the Metabolic Sites for CYP3A4-Mediated Metabolic Reactions. *Drug Metab. Dispos.* **2006**, *34*, 976–983.

(26) Olsen, L.; Rydberg, P.; Rod, T. H.; Ryde, U. Prediction of Activation Energies for Hydrogen Abstraction by Cytochrome P450. *J. Med. Chem.* **2006**, *49*, 6489–6499.

(27) Guengerich, F. P. Common and Uncommon Cytochrome P450 Reactions Related to Metabolism and Chemical Toxicity. *Chem. Res. Toxicol.* **2001**, *14*, 611–641.

(28) Shaik, S.; Kumar, D.; de Visser, S. P. Valence Bond Modeling of Trends in Hydrogen Abstraction Barriers and Transition States of Hydroxylation Reactions Catalyzed by Cytochrome P450 Enzymes. *J. Am. Chem. Soc.* **2008**, *130*, 10128–10140.
(29) de Groot, M. J.; Havenith, R. W. A.; Vinkers, H. M.; Zwaans, R.; Vermeulen, N. P. E.; van Lenthe, J. H. Ab Initio Calculations on Iron-Porphyrin Model Systems for Intermediates in the Oxidative Cycle of Cytochrome P450s. *J. Comput.-Aided Mol. Des.* **1998**, *12*, 183–193.
(30) Oda, A.; Yamaotsu, N.; Hirono, S. New Amber Force Field Parameters of Heme Iron for Cytochrome P450s Determined by Quantum Chemical Calculations of Simplified Models. *J. Comput. Chem.* **2005**, *26*, 818–826.
(31) Schöneboom, J. C.; Neese, F.; Thiel, W. Toward Identification of the Compound I Reactive Intermediate in Cytochrome P450 Chemistry: A QM/MM Study of Its EPR and Mössbauer Parameters. *J. Am. Chem. Soc.* **2005**, *127*, 5840–5853.
(32) Korzekwa, K. R.; Jones, J. P.; Gillette, J. R. Theoretical Studies on Cytochrome P-450 Mediated Hydroxylation: A Predictive Model for Hydrogen Atom Abstractions. *J. Am. Chem. Soc.* **1990**, *112*, 7042–7046.
(33) Jones, J. P.; Korzekwa, K. R. Predicting the Rates and Regioselectivity of Reactions Mediated by the P450 Superfamily. *Methods Enzymol.* **1996**, *272*, 326–335.
(34) Yin, H. Q.; Anders, M. W.; Korzekwa, K. R.; Higgins, L.; Thummel, K. E.; Kharasch, E. D.; Jones, J. P. Designing Safer Chemicals - Predicting the Rates of Metabolism of Halogenated Alkanes. *Proc. Natl. Acad. Sci. U.S.A.* **1995**, *92*, 11076–11080.
(35) Jones, J. P.; Mysinger, M.; Korzekwa, K. R. Computational Models for Cytochrome P450: A Predictive Electronic Model for Aromatic Oxidation and Hydrogen Atom Abstraction. *Drug Metab. Dispos.* **2002**, *30*, 7–12.
(36) Stewart, J. J. P. Optimization of Parameters for Semiempirical Methods II. Applications. *J. Comput. Chem.* **1989**, *10*, 221–264.
(37) Dewar, M. J. S.; Jie, C. X.; Yu, J. G. SAM1; The First of a New Series of General Purpose Quantum Mechanical Molecular Models. *Tetrahedron* **1993**, *49*, 5003–5038.
(38) Holder, A. J.; Dennington, R. D., II; Jie, C. Addendum to SAM1 Results Previously Published. *Tetrahedron* **1994**, *50*, 627–638.
(39) Frisch, M. J.; Trucks, G. W.; Schlegel, H. B.; Scuseria, G. E.; Robb, M. A.; Cheeseman, J. R.; Montgomery, J. J. A.; Vreven, T.; Kudin, K. N.; Burant, J. C.; Millam, J. M.; Iyengar, S. S.; Tomasi, J.; Barone, V.; Mennucci, B.; Cossi, M.; Scalmani, G.; Rega, N.; Petersson, G. A.; Nakatsuji, H.; Hada, M.; Ehara, M.; Toyota, K.; Fukuda, R.; Hasegawa, J.; Ishida, M.; Nakajima, T.; Honda, Y.; Kitao, O.; Nakai, H.; Klene, M.; Li, X.; Knox, J. E.; Hratchian, H. P.; Cross, J. B.; Bakken, V.; Adamo, C.; Jaramillo, J.; Gomperts, R.; Stratmann, R. E.; Yazyev, O.; Austin, A. J.; Cammi, R.; Pomelli, C.; Ochterski, J. W.; Ayala, P. Y.; Morokuma, K.; Voth, G. A.; Salvador, P.; Dannenberg, J. J.; Zakrzewski, V. G.; Dapprich, S.; Daniels, A. D.; Strain, M. C.; Farkas, O.; Malick, D. K.; Rabuck, A. D.; Raghavachari, K.; Foresman, J. B.; Ortiz, J. V.; Cui, Q.; Baboul, A. G.; Clifford, S.; Cioslowski, J.; Stefanov, B. B.; Liu, G.; Liashenko, A.; Piskorz, P.; Komaromi, I.; Martin, R. L.; Fox, D. J.; Keith, T.; Al-Laham, M. A.; Peng, C. Y.; Nanayakkara, A.; Challacombe, M.; Gill, P. M. W.; Johnson, B.; Chen, W.; Wong, M. W.; Gonzalez, C.; Pople, J. A. Gaussian 03, Gaussian, Inc., Wallingford, CT, 2004.
(40) Dennington, R., II; Keith, T.; Millam, J. Gaussview 4, Semichem, Inc., Shawnee Mission, KS, 2007.
(41) Foresman, J. B.; Frisch, Æ *Exploring Chemistry with Electronic Structure Methods,* 2nd ed.; Gaussian, Inc.: Pittsburgh, PA, 1996.
(42) Dewar, M. J. S.; Holder, A. J.; Dennington, R. D., II; Liotard, D. A.; Truhlar, D. G.; Keith, T. A.; Millam, J. M.; Harris, C. D. *Ampac 8 User Manual*; Semichem, Inc.: Shawnee, KS, 2004.
(43) Koopmans, T. The Classification of Wave Functions and Eigenvalues to the Single Electrons of an Atom. *Physica* **1934**, *1*, 104–113.
(44) Lewars, E. *Computational Chemistry: Introduction to the Theory and Applications of Molecular and Quantum Mechanics*; Kluwer Academic Publishers: London, 2003.
(45) Groves, J. T. Key Elements of the Chemistry of Cytochrome P-450. The Oxygen Rebound Mechanism. *J. Chem. Educ.* **1985**, *62*, 928–931.
(46) Shaik, S.; Cohen, S.; de Visser, S. P.; Sharma, P. K.; Kumar, D.; Kozuch, S.; Ogliaro, F.; Danovich, D. The "Rebound Controversy": An Overview and Theoretical Modeling of the Rebound Step in C-H Hydroxylation by Cytochrome P450. *Eur. J. Inorg. Chem.* **2004**, 207–226.
(47) Roy, S.; Goedecker, S.; Hellmann, V. Bell-Evans-Polanyi Principle for Molecular Dynamics Trajectories and Its Implications for Global Optimization. *Phys. Rev. E* **2008**, *77*, 056707.
(48) Jensen, F., *Introduction to Computational Chemistry*, 2nd ed.; John Wiley & Sons, Ltd.: West Sussex, England, 2006.
(49) Yoshizawa, K.; Kamachi, T.; Shiota, Y. A Theoretical Study of the Dynamic Behavior of Alkane Hydroxylation by a Compound I Model of Cytochrome P450. *J. Am. Chem. Soc.* **2001**, *123*, 9806–9816.
(50) Park, J. Y.; Harris, D. Construction and Assessment of Models of CYP2E1: Predictions of Metabolism from Docking, Molecular Dynamics, and Density Functional Theoretical Calculations. *J. Med. Chem.* **2003**, *46*, 1645–1660.
(51) Shaik, S.; De Visser, S. P., Computational Approaches to Cytochrome P450 Function. In *Cytochrome P450: Structure, Mechanism, and Biochemistry*, 3rd ed.; Ortiz de Montellano, P. R., Ed. Kluwer Academic/Plenum: New York, 2005; pp 45−85.
(52) Wang, Y.; Kumar, D.; Yang, C. L.; Han, K. L.; Shaik, S. Theoretical Study of N-Demethylation of Substituted *N,N*-Dimethylanilines by Cytochrome P450: The Mechanistic Significance of Kinetic Isotope Effect Profiles. *J. Phys. Chem. B* **2007**, *111*, 7700–7710.
(53) Wang, Y.; Yang, C. L.; Wang, H. M.; Han, K. L.; Shaik, S. A New Mechanism for Ethanol Oxidation Mediated by Cytochrome P450 2E1: Bulk Polarity of the Active Site Makes a Difference. *Chembiochem* **2007**, *8*, 277–281.
(54) de Visser, S. P.; Kumar, D.; Cohen, S.; Shacham, R.; Shaik, S. A Predictive Pattern of Computed Barriers for C−H Hydroxylation by Compound I of Cytochrome P450. *J. Am. Chem. Soc.* **2004**, *126*, 8362–8363.
(55) Carey, F. A.; Sundberg, R. J. *Advanced Organic Chemistry Part A: Structure and Mechanisms*, 4th ed.; Springer: New York, 2004.
(56) Luo, Y.-R. Comprehensive Handbook of Chemical Bond Energies; CRC Press: Boca Raton. FL, 2007.
(57) Smith, M. B.; March, J. *March's Advanced Organic Chemistry: Reactions, Mechanisms, and Structure*, 6th ed.; Wiley-Interscience: Hoboken, NJ, 2007.
(58) Karelson, M.; Katritzky, A. R.; Zerner, M. C. AM1, PM3, and MNDO Calculations of Radical Formation Energies in the Gas Phase and in Solution. *J. Org. Chem.* **1991**, *56*, 134–137.
(59) DiLabio, G. A.; Pratt, D. A.; LoFaro, A. D.; Wright, J. S. Theoretical Study of X−H Bond Energetics (X = C, N, O, S): Application to Substituent Effects, Gas Phase Acidities, and Redox Potentials. *J. Phys. Chem. A* **1999**, *103*, 1653–1661.
(60) Klein, E.; Lukes, V.; Ilcin, M. DFT/B3LYP Study of Tocopherols and Chromans Antioxidant Action Energetics. *Chem. Phys.* **2007**, *336*, 51–57.

CI8003946